Published in IBPSA World News, Volume 30, No. 2, pp. 29 – 41 (October 2020)
www.ibpsa.org/Newsletter/IBPSANews-30-2.pdf

SITE-SPECIFIC WEATHER FILES AND FINE-SCALE PROBABILISTIC MICROCLIMATE ZONES FOR CURRENT AND FUTURE CLIMATES AND LAND USE

(for energy modeling, analysis, forecasting, and LEED **)**

Haider Taha
Altostratus Inc.
haider@altostratus.com -- www.altostratus.com

A. Preamble

It is well-known that urban areas, depending on extents and physical / geometrical characteristics, create distinct climates and intra-urban microclimate variabilities that are typically very significant and sometimes of the same magnitude as inter-regional differences in climate (Taha 2017, 2015a,b, 2020a,b). These intra-urban variations can significantly affect energy use, thermal environmental conditions, heat-health, emissions, and air quality (Taha 2017). Translating climate effects into energy-use equivalents and developing weather files to account for these effects is an on-going endeavor pursued across the industry, research, and academic spectrum, e.g., Crawley (2007); Huang (2010, 2016); Hong et al. (2016, 2017); Dickinson and Brannon (2016); Bueno et al. (2011); Jentsch et al. (2015); New et al. (2018); Nair et al. (2020); and Mylona et al. (2012), among others.

Accurate, site-specific microclimate characterizations are critical in the design of new buildings or retrofits; in building code or certification compliance; in testing building performance under a range of weather conditions; and in deploying energy technologies that will be equally effective in current and changing climates (Herrera et al. 2017; Alfaro et al. 2004; Taha 2015a,b; de Wilde and Coley 2012). Currently, however, most weather input to building energy models does not explicitly take into account the effects of such fine-scale intra-urban variations or the specific micrometeorological fields at a site of interest.

Existing climate zones are also generally coarse, regardless of the application, e.g., energy, public health, or emissions / air-quality, since they are based mostly on airport weather data, despite recent increases in observations from mesonets and urbanets. By comparison, significant intra-urban variability in microclimates occurs at much finer scales, e.g., sub-kilometer and sub-hourly (Taha 2008a,b,c, 2017; Taha et al. 2018a,b). For example, Taha (2020a) shows that the current California Building Climate Zones (BCZ) are too coarse and that intra-urban variability in microclimates can be so large that it is possible in effect to create within each BCZ a number of temperature subzones (e.g., ~5 km length scales) with *intra*-zone temperature gradients similar to or larger than the *inter*-zone gradients of the coarse BCZ sometimes by several folds (Figure 1).

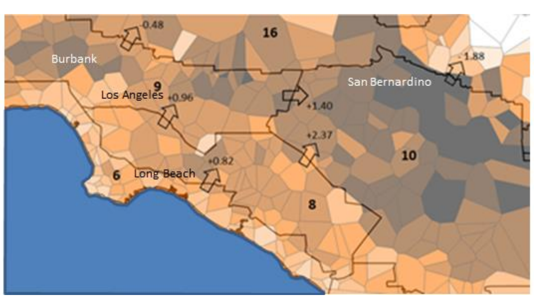

Figure 1: Los Angeles region fine-scale temperature zones (color-coded) produced by Altostratus Inc. (Taha 2020a) vs. California Building Climate Zones (BCZ), numbered. In this example, the Altostratus zones are based on synthetic observational August (2013-2015); each step change in color is 1.2 °C.

For current climate, Altostratus Inc. develops these probabilistic fine-scale intra-urban microclimate zones based on both observations (from mesonet and urbanet) and high-resolution atmospheric model fields. For future climates, the microclimate zones are developed based on dynamically-downscaled climate fields that are locally enhanced with the Altostratus-modified uWRF model (discussed below). In both cases, a clustering technique (Taha 2020a) is used to create zones based on their spatial properties, extents, and persistence across specified time intervals (e.g., a specific month across N years) or ensembles of N simulation members, etc. For each area, a length scale analysis is applied for every desired period and scenario creating a union of N initial zones (at each location) that are superimposed (Figure 2, is an example where N = 3). These N initial zones vary spatially across the months, years, or scenarios. With spatial analysis and pattern recognition (GIS), these initial zones can then be decomposed into persistent (intersection of all N initial zones), semi-persistent (n intersections, where n < N), and inconsistent initial zones (no intersections) (Taha 2020a).

Figure 2: Development of characteristic temperature zone from N initial zones, e.g., N-member ensemble or N years, etc. In this example, N = 3 (source: Taha 2020a)

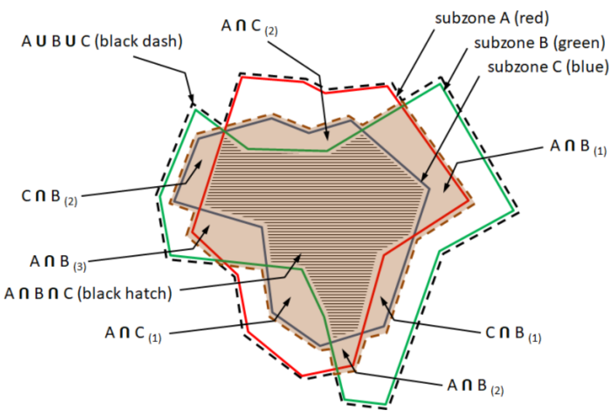

The union and intersection processes to generate a characteristic zone are explained schematically in Figure 2, using three hypothetical initial zones A, B, and C, in this example. In this figure, the union of initial subzones is delineated with the black dashed line. Thus, in this case, with N = 3, the resulting final zone is defined as:

$$[A \cap B \cap C] + A \cap B_{(1)} + C \cap B_{(1)} + A \cap B_{(2)} + A \cap C_{(1)} + A \cap B_{(3)} + C \cap B_{(2)} + A \cap C_{(2)}$$

The first term (in brackets) represents the hatched area (in Figure 2), which is the equivalent of what was defined above as a "persistent" initial zones, and the remaining seven terms of the equation represent the individual brown-colored parcels surrounding the hatched area (in this example, clockwise from top right). Thus, the final probabilistic zone is delineated with the dashed brown line (intersection of N = 2) and is shown in brown (including both the brown hatch area and non-hatch brown area). This process is repeated for all locations in an area of interest (e.g., Figure 1) where the length scale analysis is carried out and for all regions and time periods (and scenarios) in current and future climates.

These issues also pertain to the evaluation of future climate effects on energy use, e.g., heat exacerbation and weather patterns (Fann et al. 2016; Houghton and English 2014; Taha 2017, 2020a,b). As urban areas exacerbate regional warming (Taha 2017; Founda and Santamouris 2017), there is an increased emphasis on the need to account for fine-scale climate variations within urban areas and consider these issues as priority research in developing projections of future climate impacts (Hess et al. 2018; Ebi et al. 2018; Cheng and Berry 2013). This is one reason why the changes in climate zones (under future climate and land-use conditions) also need to be characterized.

B. Weather products

For various applications, Altostratus Inc. has been developing methodologies to create high-resolution meso-urban weather data based on advanced, fine-scale urbanized atmospheric modeling and observations. Altostratus can create site-specific weather files for any location under current and future climates and their corresponding urbanization levels and land-use characteristics. The simulations are carried out specifically and explicitly for the desired site, not merely extracting model output at specified locations as a post-processing step.

For energy applications, Altostratus applies state-of-science methodologies, datasets, and advanced atmospheric models to create (1) fine-scale probabilistic microclimate zones (as shown in Figure 1, for example) and (2) site-specific weather data for energy forecasting, planning, and analysis. Based on meteorology and land-use characteristics, each microclimate zone's spatial extents (length scales) are dynamically determined. The fine-scale microclimate zones also vary in spatial extents and properties, e.g., on a decadal time scale, to capture effects of changes in climate and emissions (RCP), land use, surface physical properties, emissions and exacerbation of heat, implementation of control measures and policies, deployment of renewable energy technologies, and fleet electrification. Thus, sets of microclimate zones are developed to reflect various possible scenarios.

Enhanced site specificity of weather files, e.g., for a particular building location, is achieved with modeling at resolutions of 200 m and finer while accounting for (1) the effects of the site's urban morphometric characteristics, land cover, surface physical properties, and sources of heat, (2) effects of physical properties of the site's surroundings, and (3) characteristics of upwind areas within meteorological radii of influence, i.e., per dynamically-determined, wind-direction-dependent, time-varying length scales. The methodology is fully site-specific based on in-situ bottom-up surface and canopy-layer characterizations, advanced urban parameterizations, fine-scale prognostic modeling including observational data assimilation and variational analysis, bias-corrected dynamical downscaling of climate models (for future years), and physical characterizations of projected urbanization corresponding to the downscaled future timeframes of interest.

C. Model performance evaluation

An important aspect in these activities is to thoroughly demonstrate model performance following any meteorological-model update, customization, and modification. Over the years, Altostratus has provided a detailed summary of model performance that accompanies each study and project report to ensure full acceptability of results. Model performance is compared against community-recommended benchmarks (e.g., Emery et al. 1997; Tesche et al. 2001; Taha 2017) at each weather station in the domain of interest. Rigorous statistical performance evaluation includes using metrics such as bias, gross error, root mean square error, index of agreement, time series, maxima / minima, and ranges as applicable to each variable such as temperature, relative humidity, wind speed, wind direction, heat and moisture fluxes, and others as needed.

One such example is shown in Figure 3 depicting improved temperature forecast skill (model performance) in the Los Angeles and San Francisco Bay Area regions resulting from using the Altostratus-modified uWRF (Taha 2017, 2020a,b) relative to the standard WRF model (Section D.3). This example is from a study performed by Altostratus Inc. for the California energy commission (Taha 2020a). For the random sample shown (July 16-31, 2013), model performance in the Los Angeles region improved significantly at 225 stations (green-coded circles) but worsened at 6 stations (red-coded circles). In the San Francisco Bay Area (SFBA), model performance improved significantly at 150 stations but worsened at 10 stations. The mean error was reduced by up to 1.8 °C (46%) in SFBA and up to 0.8 °C (33%) in the Los Angeles region. Furthermore, Taha (2017, 2020a,b) and Taha et al. (2018a,b) showed that the Altostratus Inc. modifications in uWRF significantly improved performance not only with respect to standard, non-urban WRF, but also with respect to the standard WRF-urban model (Chen et al. 2010).

Figure 3: Los Angeles region (L) and San Francisco Bay Area (R) mesonet stations (circles) and current BCZ boundaries (yellow lines). The circles are color-coded to indicate improvements in model performance with the Altostratus-modified uWRF at each station relative to the standard WRF modeling approach. The squares are metars and existing weather-file locations (EPW). Source: Taha (2020a).

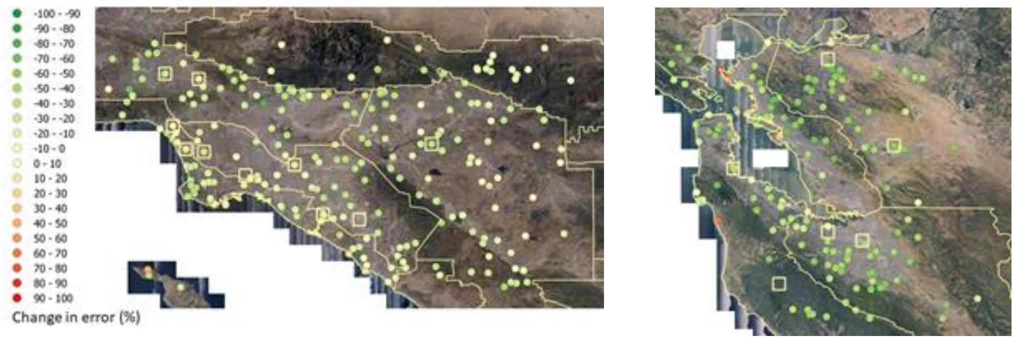

D. Methodology

In the following sections, a very brief, high-level overview of the methodology in the context of an example domain (Sacramento Valley, California) is presented. This is a domain for which a number of weather files are made available for evaluation. To conserve space in this short article, references to some data sources are not provided in the discussion items below – they can be made available upon request. The end product of the approach discussed here is to develop modified meteorological fields input to the EnergyPlus program (Crawley et al. 2001), but of course can be used with any other building energy model.

Figure 4: Forecast 2-m air temperature for 2000 PDT, March 16, 2020 (produced by Altostratus Inc.-modified uWRF). Circles are locations of mesonet stations.

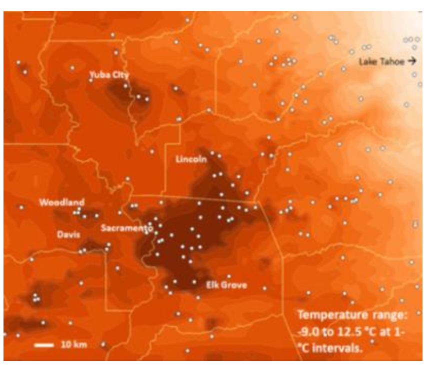

D.1 Observational weather analysis

Altostratus obtains hourly and sub-hourly observational weather data from the MADIS system and other sources, if needed, including: Urbanet; National Weather Service Coop; WeatherBug; NOAA MesoWest; NCAR datasets; California Irrigation Management Information System (CIMIS); and network-specific California datasets, e.g., ARB and AQMDs. Hourly data from weather-station networks (e.g., white circles in Figure 4 for the Sacramento area) are used in: (1) characterizing the current intra-urban microclimate variations, albeit at coarser resolutions than is possible with the atmospheric model, (2) developing microclimate zones in the selected regions (as discussed in Section A), which also guides the modeling effort, (3) developing the reference benchmarks for subsequent use in model performance evaluation, and (4) developing the input to 4-dimensional data assimilation schemes in the meteorological model.

D.2 Land use / land cover (LULC) and surface characterization

Detailed LULC analysis is done to supplement other data sources and derive / develop surface physical properties input to the meteorological / land-surface models. A detailed, area-specific, bottom-up approach (Taha 2008b, 2017, 2020a,b; Taha et al. 2018a) is used to characterize the physical and geometrical properties of the surface, especially in urban areas, based on data sources including: 30-m National Land Cover Data and impervious cover; 30-m USGS Anderson Level-II and Level-IV land use; Google Earth PRO urban morphological and land-cover data; 1-m aerial imagery-based roof and pavement albedo; 1-m area-specific LiDAR-derived urban morphological and geometrical data (including N/WUDAPT); 1-m EarthDefine/CALFIRE urban tree canopy cover; and 30-m MRLC / USFS canopy cover and MODIS albedo.

Taha (2008a,b,c, 2017, 2020a,b) developed a methodology to derive area- and site-specific urban morphometric, geometrical, and surface physical properties from Google Earth PRO in conjunction with other sources of LiDAR data. As shown in Figure 5A,B, for example, this information is converted from Google Earth PRO (5B) into various parameters for each model computational volume (5A) in the canopy and boundary layers.

Figure 5: **A:** High-resolution vertical levels (2 – 5 m) in the urban canopy model. **B:** Characterization of 3-D urban morphology in Google Earth PRO. **C:** Current urban areas (green) and projected urban growth by 2050 (pink) in the greater Sacramento Valley, California, region (Taha 2020b).

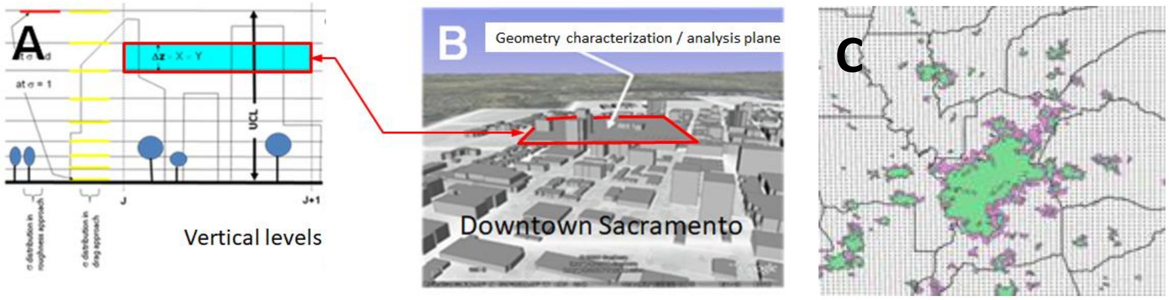

For future years, e.g., through 2100, several LULC-projection datasets exist, including the USGS Land Use and Carbon Scenario Simulator (LUCAS) (Sleeter et al. 2017a,b). Altostratus has vectorized and used the LUCAS data to develop future-year projections (e.g., for year 2050, as in Figure 5C) and characterize urbanization changes to derive surface physical properties. In this context, Taha (2017, 2020a,b) developed a methodology to extrapolate the current LULC makeup and surface physical properties near the growth boundaries to nearby future urbanizing areas. These characterizations are also subsequently used in dynamical downscaling of climate models.

D.3 Atmospheric modeling of current climate and land use

For the purpose of urban atmospheric modeling, several mesoscale meteorological models, such as the Weather Research & Forecasting model, WRF (Skamarock et al. 2008) have been enhanced with urban parameterizations that improve the representation and quantification of urban canopy- and boundary-layer processes and more accurately quantify the urban influences on the atmosphere (Martilli et al. 2002; Chen et al. 2010; Salamanca and Martilli 2009; Kusaka et al. 2001; Taha 2008a,b,c; Fan and Sailor 2005).

At Altostratus Inc., Taha (2008a,b,c, 2015a,b, 2017, 2020a,b) has further refined the WRF urban parameterizations and their applications and developed more advanced techniques and a modified version of the urban WRF model (referred to as “uWRF” in this article). The refinements allow for very fine-scale specification of surface physical properties in the model, ability to characterize the 3-dimensional properties of urban areas in detail (e.g., down to street scale), and an accurate quantification of the sources of heat in each area, all of which improves the model’s calculations of various prognostic variables. The refinements also improve upon existing urban surface-characterization techniques, such as WUDAPT (Ching et al. 2009), in that each grid cell in the domain can be independently and directly characterized based on remote-sensed information and ground-based surveys (e.g., Taha et al. 2018a,b) instead of using land-use as a generic proxy, which is the current approach. The urban canopy-layer models in WRF are also modified and improved by Taha (1999, 2017, 2020a,b) including how the urban parameterizations are called (triggered) per physics criteria (applied independently at each grid cell), including turbulent kinetic energy, heat storage, anthropogenic heat emissions, and urban morphology, thereby replacing the existing approach which is based on land-use type. All of these improvements help achieve more accurate location-specific microclimate simulations and, thus, more accurate quantification of the effects of intra-urban variability in climate and surface physical properties on energy use.

For current climate, reanalysis is used to provide boundary conditions to the meteorological model. Observations from mesonet and metar are also assimilated into the model. Both deterministic and probabilistic (e.g., ensemble) simulations are carried out.

D.4 Atmospheric modeling of future climates and land use

The local future microclimates (e.g., for the example domain) are characterized via (1) dynamically-downscaling a bias-corrected CMIP5 model -- CCSM4, Community Climate System Model (Bruyere et al. 2014; NOAA 2015) and (2) highly-urbanized meteorological modeling at the sub-kilometer and sub-hourly scales using the Altostratus-modified uWRF (Taha 2008a,b; Taha 2017). Future years, RCP scenarios, and future land-use projections are modeled to develop an ensemble of simulations that captures potential local impacts of future climate and develop probabilistic microclimate zones and future site-specific forecasts.

The development of future microclimate zones does not only account for the effects of changes in climate (via dynamical downscaling) but also (1) changes in land use / urbanization, (2) changes in heat and pollutant emissions and impacts on radiative forcing, and (3) implementation of selected regional measures and policies including solar PV, cool communities, fleet electrification, and distributed generation and renewables.

E. Example geographical domain and sample weather files

The example domain (greater Sacramento Valley, California), is shown in Figure 6A (red rectangle) and magnified in Figures 6B, 6C. The central part of this domain is relatively homogeneous, mostly flat with no major water bodies, devoid of abrupt topographical features, except for the gradual upslope towards higher elevations near the eastern edge of the domain. Thus the bulk of intra-urban microclimate variations are caused by changes in surface characteristics and heat transport along the air-mass trajectories over urban areas (Figure 6C) (Taha 2020b).

In the following discussion, two random urban locations are compared to Sacramento Executive airport (hereafter called “EXEC” for short) which is the source of TMY3 data in an existing weather file. The two locations are:

1. An AB-617 community “B”, one of ten disadvantaged areas identified by the Sacramento Metropolitan Air Quality Management District (SMAQMD). This will be referred to as “AB” in the following discussion and is 12 km NNE of EXEC. It is identified with a green circle in Figure 6B, 6C.
2. A location in the City of Citrus Heights, referred to as “CTRS” in this discussion, and is 25 km NE of EXEC. It is identified with a yellow circle in Figure 6B, 6C.

For the whole region, there are only two weather files (TMY#) currently in use: one at Sacramento Metro AP and one at Sacramento Executive AP (two red circles in Figure 6B). The white circles are random urban locations for which Altostratus generated sample weather files for current and future climates and land use. The files are currently *.csv-formatted for EnergyPlus (*.epw) and the file names are listed along with the locations in Figure 6B (zooming on the figure is necessary to see the file names).

The sample weather files are for years 2019 and 2050 (RCP 8.5). Using the same methodology described in Section D, Altostratus can generate weather files for any location worldwide and any time horizon (past, current, and future) per a user’s interest. The future-climate scenarios produced by Altostratus, such as the 2050 RCP 8.5 samples provided here, also account for the effects of changes in land use and land cover, and urbanization tendencies (projected) by the year 2050, not just the changes in climate.

In order to provide the user with different options for applying the fine-scale model and observational weather data (for both current and future climates), the products are made available as:

Option 1: Model perturbations applied to current weather files (TMY / EPW for example) via departures from monthly means (indirect mapping) or hour-to-hour departures (direct mapping). This results in *synthetic* weather files, meaning that they are modifications to current TMY data. Conceptually, for a variable *V*, this can be described as:

$$V_{TMY} = \overline{V}_{TMY} + V'_{TMY} \; ; \quad V_{uWRF} = \overline{V}_{uWRF} + V'_{uWRF} \; ; \quad \textbf{\textit{and}}: \; V_C = \overline{V}_{TMY} + V'_{uWRF}$$

where V_c is the desired computed value of the variable (the equations are generic, i.e., they can be applied in space or in time, as well as both simultaneously). This option allows users of existing weather data (e.g., TMY) to directly evaluate the improvements in and intra-urban spatiotemporal enhancements to meteorological fields in TMY (resulting from the Altostratus methodology) in a region of interest and to directly compare them to the existing weather files;

Option 2: Model perturbations applied to observational data from metar and other high-quality weather stations, e.g., from NOAA. This no longer produces a *synthetic* weather file as compared to option 1 and is more realistic because the observations come not from a composite weather file (e.g., TMY) but, rather, from dynamically-consistent hourly and sub-hourly observations for a specific time interval, e.g., a full year; and

Option 3: Absolute model fields (whether deterministic or probabilistic) at any and all locations of interest for the desired periods. In this case, the fields are absolute, dynamically consistent, and no longer based on departures from some spatial or temporal means, such as from existing weather files.

In all options, the modified variables of most relevance to the EnergyPlus program (Crawley et al. 2001) are *DBT*, *DEW*, *RH*, *SW*, *DIFF*, *LW*, and *WSP*, discussed further below and defined in Figure 9.

Option 3 is the most correct, scientifically-sound approach, and the one recommended for use. However, all three options can be made available to interested parties if so desired. Although rarely the case, option 1 can result in unrealistic values at times. For example, in the sample data provided and discussed below, this option can produce temperatures in 2050 RCP 8.5 that reach 50 °C during a few hours in the year (outliers). In the datasets discussed below, examples from options 1 and 3 are provided.

For parties interested in testing sample weather data, Altostratus is making available fine-scale weather files for current and future climates. These samples are currently for the Sacramento Valley, California (Capital region), for the locations shown in Figure 6B, and can be accessed via ftp. If interested in obtaining test weather files or in generating weather data for other time periods, regions, specific communities, selected neighborhoods, or specific building sites, Altostratus can provide additional information.

In the following discussion, locations EXEC, AB, and CTRS are compared. As space is limited in this short article, only air temperature comparisons are shown in somewhat larger graphics in Figure 7 and summarized with additional information in Figure 8. For other variables, postage-stamp graphs are shown in Figure 9 to provide a general idea. In all graphs, the red ellipses represent the bivariate normal density, provided here merely as a visual aid to discern outliers or extreme values in the data from 8760 hours, in respective years, and the red line is the identity line.

In general, the graphs in Figures 7, 8, and 9 can be grouped into two sets: (1) those representing spatial comparisons, i.e., comparing variables at different locations but for the same timestamps and (2) those representing temporal comparisons at different timestamps (e.g., across different years) but at the same respective locations. Thus one observation that can be made is that the spatial comparisons (graphs A1, A2, D1, and D2 in Figure 67 and rows R1, R2, R7, and R8 in Figure 9) have a smaller scatter than the temporal comparisons. This is expected since the spatial variations during a timestamp over relatively small distances are likely smaller than comparing, say, a certain hour in current and future climates.

Graphs A1 and A2 (in Figure 7) are from option 1 (for current climate, 2019) and show dry-bulb temperature increasing away from EXEC location because of intra-urban heat transport (as explained by the trajectories in Figure 6C). Because of that, AB has a net increase of 5190 °C·hr yr^{-1} relative to EXEC, whereas CTRS has a net increase of 8157 °C·hr yr^{-1} relative to EXEC. The annual all-hours temperature average at EXEC, AB, and CTRS are 15.55, 16.14, and 16.48 °C (Figure 8). Thus, over a relatively short distance between these stations, an annual-average 1 °C difference can result because of intra-urban microclimate effects, which is very significant. The largest increases in temperature relative to EXEC occur during the mid-ranges of absolute temperature and can be as much 4 °C warmer in AB and up to 6 °C warmer in CTRS at any given hour within that temperature range. This can also be seen in graphs A1 and A2 (entasis) as well as in the upward shift of the interquartile ranges seen in Figure 8, A1 and A2, where the 1st quartile is relatively unchanged but the 3rd quartile is higher.

Figure 6. **A**: Sample domain (red rectangle). **B**: Locations of sample weather files available for testing. Red circles are existing TMY/TMY3 *EPW weather data for the region (Sacramento Metro and Sacramento Executive airports). White circles are locations of sample Altostratus Inc. weather files in urban areas. Green and yellow circles are AB and CTRS locations, respectively. **C**: Back-trajectories arriving Rocklin area at 1400 PDT on 13 different days during the interval July 16 – 31, 2015. The "4" markers show the air-mass position four hours prior to arriving at Rocklin (Taha 2020b). Zooming into Figure B can help identify file names.

Graphs B1, B2, ad B3 (in Figure 7) are spatial comparisons based on option 1, but for the year 2050 (RCP 8.5). Thus, B1 is EXEC in 2050 relative to TMY3, B2 is AB in 2050 vs. AB in 2019, and B3 is CTRS in 2050 relative to CTRS in 2019. The net warming (from 2019 to 2050) at EXEC is 8649 °C·hr yr^{-1} (or 0.99 °C·hr hr^{-1}), at AB the net warming is 9187 °C·hr yr^{-1} (or 1.05 °C·hr hr^{-1}), and at CTRS, it is 10321 °C·hr yr^{-1} (or 1.18 °C·hr hr^{-1}). Indeed, the climate-model fields downscaled via Altostratus uWRF suggest that the warming (relative to present conditions) increases in the NNE and NE directions in this region. This can also be seen in differences B1, B2, and B3 in Figure 8.

Graph C1 (in Figure 7) is a temporal comparison between absolute model fields at EXEC in 2019 vs. TMY3. That is, the graph shows hour-to-hour comparisons between the model's absolute output for year 2019 versus TMY3 at EXEC, hence the relatively large scatter. The model year 2019 shows a net warming (relative to TMY3) of 8722 °C·hr yr^{-1} (or almost 1.0 °C·hr hr^{-1} as an annual average – also see difference C1 in Figure 8). The next two graphs are spatial comparison at AB (D1) and CTRS (D2), relative to EXEC, all based on absolute meteorological model output for 2019. Thus this is a more dynamically-consistent set of data that can be inter-compared directly. In this case, AB sees a net warming of 5187 °C·hr yr^{-1} (or 0.59 °C·hr hr^{-1} over 8760 hours) relative to EXEC, whereas as CTRS sees net warming of 8149 °C·hr yr^{-1} (or 0.93 °C·hr hr^{-1}) relative to EXEC (also see Figure 8, differences D1 and D2).

Finally, graphs E1, E2, and E3 (Figure 7) show a comparison of year 2050 vs. 2019 at each respective location (EXEC, AB, and CTRS), all from model results (absolute fields, not perturbations). Thus, again, this is a dynamically-consistent set of variables that can be useful to compare. The differences at each location were already used above and mapped onto existing conditions to generate synthetic weather files, as seen in graphs B1, B2, and B3 (Figure7). Thus, these are again local net warmings of 0.99 °C·hr hr^{-1}, 1.05 °C·hr hr^{-1}, and 1.18 °C·hr hr^{-1} at EXEC, AB, and CTRS, respectively, as annual averages (over 8760 hours). The differences can also be seen in Figure 8 (E1, E2, and E3).

In all of the above analysis, one should keep in mind that CTRS, relative to EXEC, is not even at the downwind-most end of the trajectories shown in Figure 6C. Thus, for other locations further downwind, such as those to the N, NE, and E of CTRS (the yellow circle in Figure 6B,6C), the differences (i.e., warming) relative to EXEC are even larger.

To wrap up this discussion, the absolute model fields for current climate (2019) and future year (2050) are compared with the TMY3 weather file for EXEC (Sacramento Executive Airport). This is to give the TMY3 user a sense of how different the building energy simulations and calculations could be if the actual 2019 year were used instead of the composite TMY3 and also how modeled future years compare to present. To do that, the last 6 datasets in Figure 8 are compared to TMY3 (the first dataset on the left in Figure 8).

Relative to TMY3 (at EXEC), the 2019 all-hours average temperature at EXEC is 0.99 °C higher – at AB it is 1.58 °C higher (than TMY3) and at CTRS it is 1.92 °C higher (than TMY3). The 2050 all-hours averaged temperature at EXEC is 1.98 °C higher than TMY3, at AB it is 2.63 °C higher (than TMY3), and at CTRS, it is 3.10 °C higher (than TMY3). Since these are annual averaged differences (over 8760 hours), they are quite significant. Finally, it can also be stated that the intra-urban differences in temperature, caused by urban heat transport along trajectories (Figure 6C) and local heat generation / surface properties, is of the same magnitude as the predicted local effects of climate change (in 2050, in this example). Spatially, in 2019, AB is warmer than EXEC by an annual average of 0.59 °C and CTRS is warmer than EXEC (in 2019) by an annual average of 0.93 °C (these spatial differences are based on model results). The changes in climate and land use produce a local warming of 1.05 °C at AB (in 2050 relative to 2019) and a warming of 1.18 °C at CTRS (in 2050 relative to 2019). Thus comparing 0.59 °C (spatial) to 1.05 °C (climate) and 0.93 °C (spatial) to 1.18 °C (climate) shows that the spatial impacts of intra-urban microclimate variations are of the same magnitude as the local predicted impacts of climate change between now and 2050 (RCP 8.5).

Of course, all of these comparisons and findings are specific to this region, selected locations, and years / scenarios. Other regions, time horizons, or scenarios, will likely yield different results. Hence, it is important to carry out the modeling and forecasting on an area- and site-specific basis, which is the main argument in the approach presented in this article.

Finally, Figure 9 summarizes the same type of analysis but for other meteorological variables. In this figure, rows R1 through R11 are defined as follows (y-axis vs. x-axis):

R1: AB vs. TMY3 (option 1); **R2**: CTRS vs. TMY3 (option 1); **R3**: EXEC 2050 vs. TMY3 (option 1); **R4**: AB 2050 vs. AB 2019 (option 1); **R5**: CTRS 2050 vs. CTRS 2019 (option 1); **R6**: EXEC 2019 vs. TMY3 (option 3); **R7**: AB 2019 vs. EXEC 2019 (option 3); **R8**: CTRS 2019 vs. EXEC 2019 (option 3); **R9**: EXEC 2050 vs. EXEC 2019 (option 3); **R10**: AB 2050 vs. AB 2019 (option 3); and **R11**: CTRS 2050 vs. CTRS 2019 (option 3). The options were defined at the beginning of Section E.

In this figure, DEW is in °C, DIFF, LW, and SW are in W m^{-2}, RH is in %, and WSP is in m s^{-1}.

Figure 7: Comparisons of various temperature indicators at EXEC, AB, and CTRS.

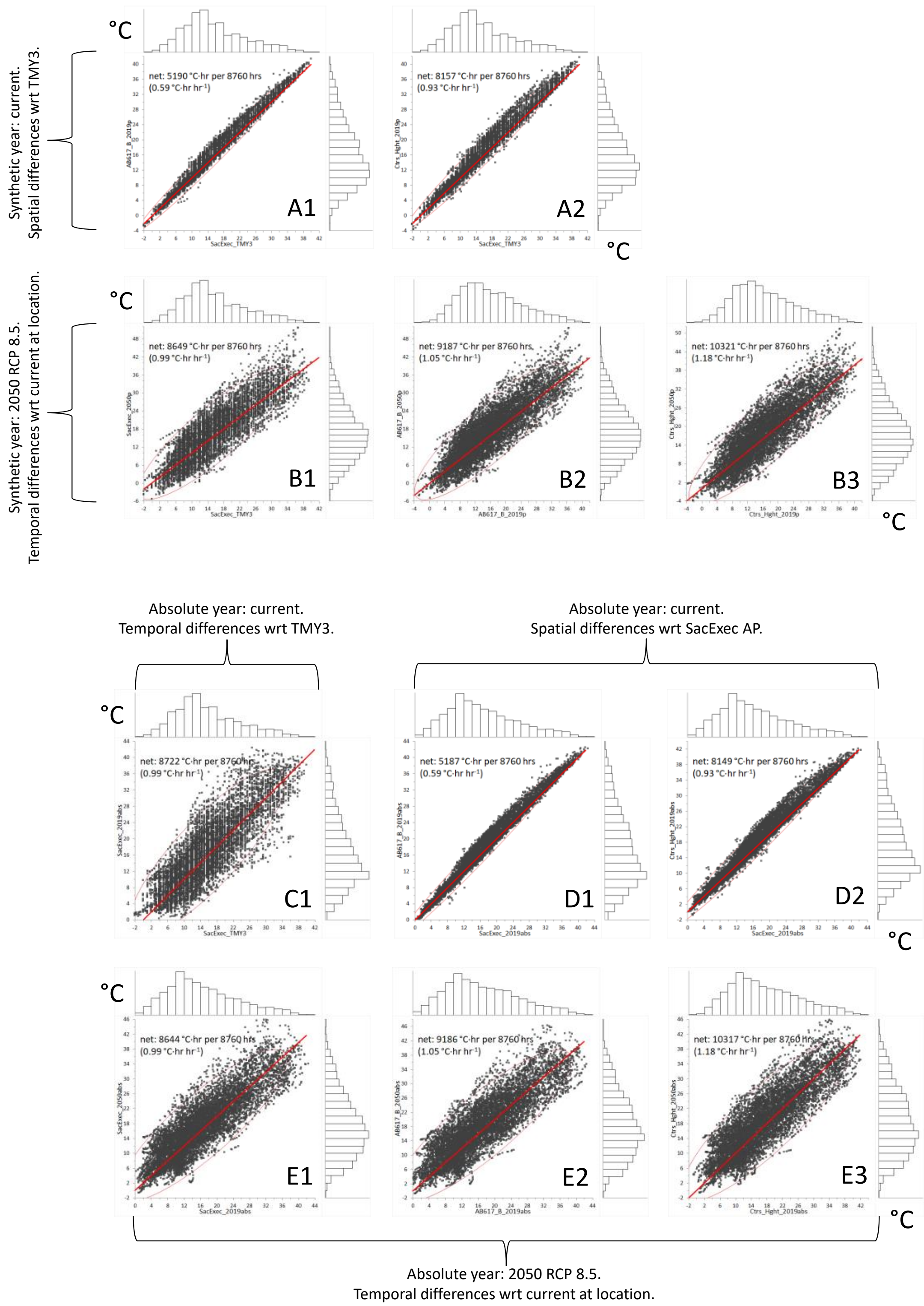

Figure 8: Descriptive statistics for 8760 hours of air temperature at EXEC, AB, and CTRS. At the bottom of the figure, differences are labeled for cross-referencing to graphs in Figure 7.

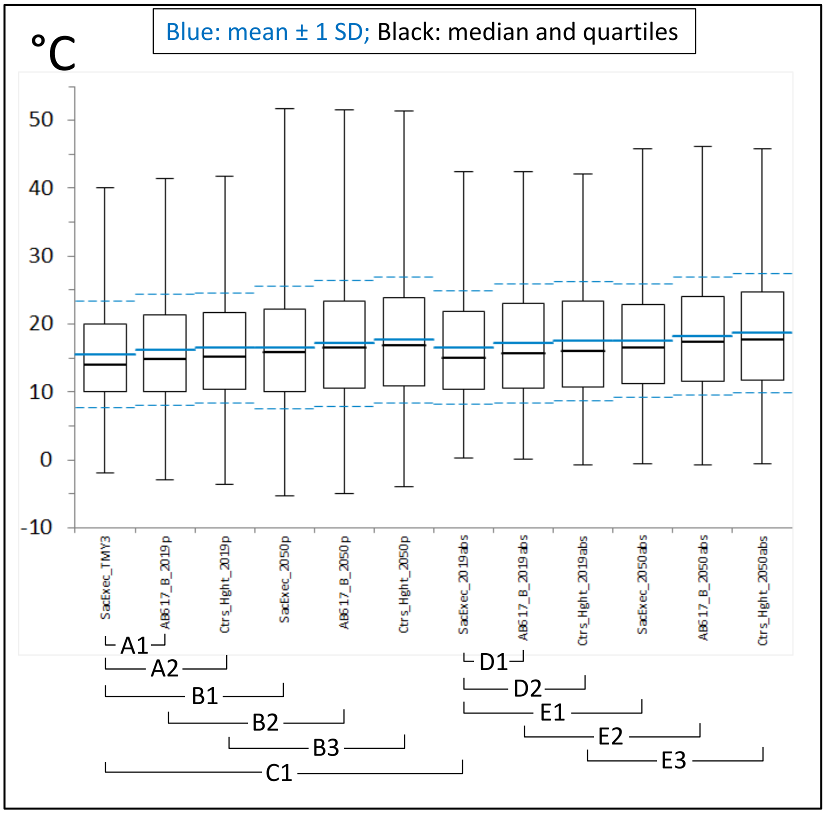

[Figure 9 follows on page 12]

DATA ACCESS AND DISCLAIMER

The sample weather files for the Sacramento Valley, California, domain shown in Figure 6B can be obtained from Altostratus Inc. via FTP. Please contact us for access information.

These weather files are made available for testing purposes only. They are not intended for commercial use or application to on-going projects. Altostratus Inc. is not responsible for any outcome resulting from use of these sample weather files. If interested in applying such data to on-going projects or in creating new ones for your location, please contact Altostratus Inc.

A "README" note is also provided on the FTP site with additional information on the files and their corresponding locations in the domain.

Figure 9: Selected comparisons among variables. **DEW**: dewpoint; **DIFF**: diffuse radiation; **LW**: longwave radiation from sky; **RH**: relative humidity; **SW**: direct normal radiation; **WSP**: wind speed.

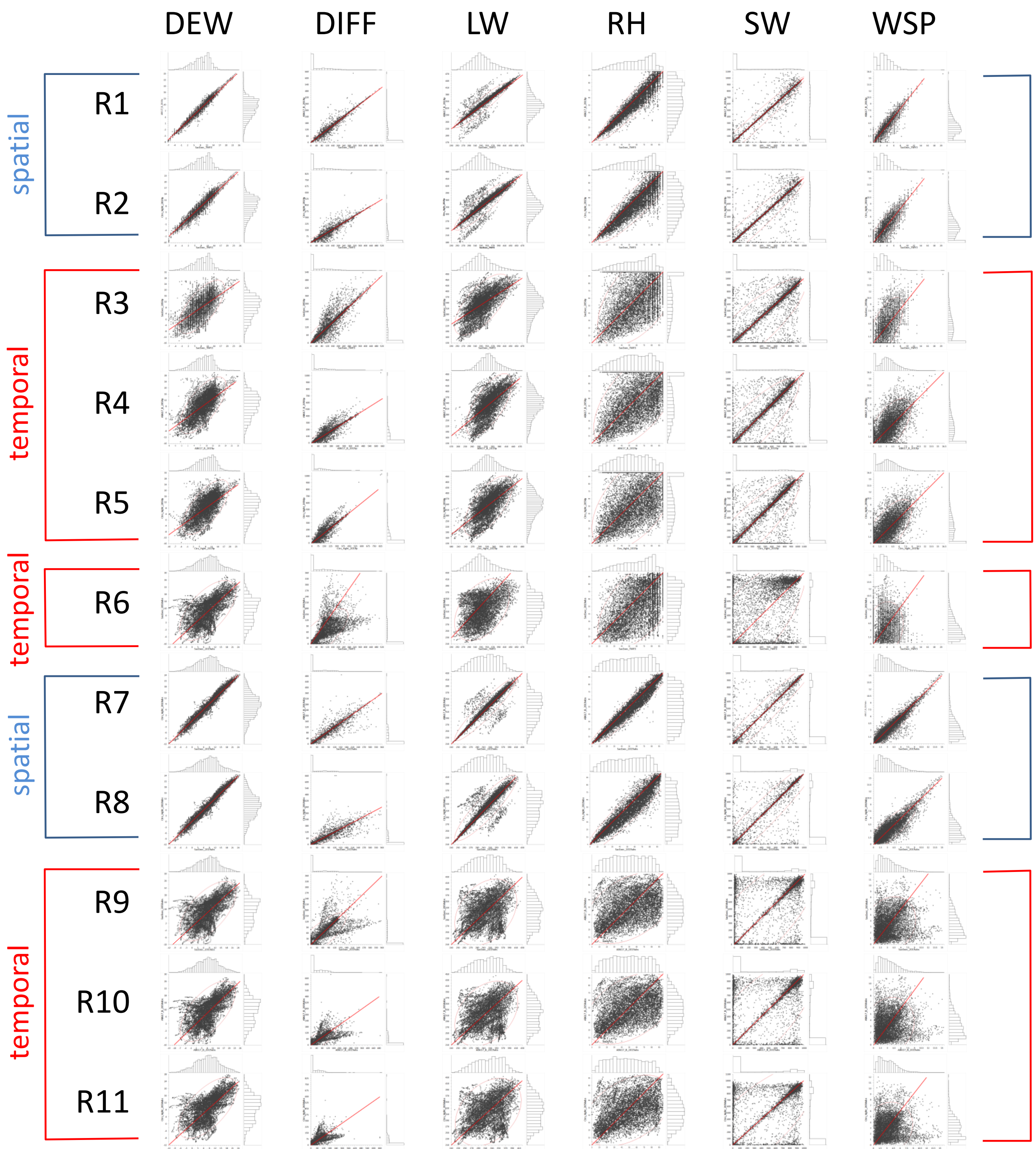

REFERENCES

Alfaro E, Gershunov A, Cayan D, Steinemann A, Pierce D, Barnett T, 2004. A method for prediction of California summer air surface temperature, EOS Transactions AGU, 85, 553–558 doi:10.1029/2004EO510001.

Anderson JR, Hardy EE, Roach JT, Witmer RE, 2001. A land use and land cover classification system for use with remote sensor data. USGS Professional Paper 964, U.S. Government Printing Office, Washington, DC.

Bueno B, Norford L, Pigeon G, Britter R. 2011. Combining a detailed building energy model with a physically-based urban canyon model. Boundary-layer meteorology, 140, 471-489, doi: 10.1007/s10546-011-9620-6.

Chen F, Kusaka H, Bornstein R, Ching J, Grimmond CSB, Grossman-Clarke S, Loridan T, Manning K, Martilli A, Miao S, Sailor D, Salamanca F, Taha H, Tewari M, Wang X, Wyszogrodzki A, Zhang C, 2010. The integrated WRF/urban modeling system: development, evaluation, and applications to urban environmental problems. International Journal of Climatology doi:10.1002/joc.2158.

Cheng JJ, Berry P, 2013. Development of key indicators to quantify the health impacts of climate change on Canadians. International Journal of Public Health, 58, 765-775, doi: 10.1007/s00038-013-0499-5.

Crawley DB, 2007. Creating weather files for climate changes and urbanization impacts analysis. Proceedings of Building Simulation 2007, IBPSA, Beijing, China.

Crawley DB, Lawrie LK, Winkelmann FC, Buhl WF, Huang YJ, Pedersen CO, Strand RK, Liesen RJ, Fisher DE, Witte MJ, Glazer J, 2001. EnergyPlus: creating a new-generation building energy simulation program, Energy and Buildings, 33, 319-331, doi: 10.1016/S0378-7788(00)00114-6.

deWilde P, Coley D, 2012. The implications of a changing climate for buildings. Building and Environment, 55, 1-7 doi:10.1016/j.buildenv.2012.03.014.

Dickinson R, Brannon B, 2016. Generating future weather files for resilience. 36th International Conference on Passive and Low Energy Architecture. Cities, Buildings, People: Towards Regenerative Environments, July 11-13 (2016), Los Angeles, California.

Ebi KL, Boyer C, Bowen KJ, Frumkin H, Hess J, 2018. Monitoring and evaluation indicators for climate change-related health impacts, risks, adaptation, and resilience. International Journal of Environmental Research and Public Health, 15, 1943, doi: 10.3390/ijerph15091943.

Emery C, Yarwood G, Heiken J, Tran C, 1997. Air quality modeling evaluation of the "Cool communities" ozone control strategy. Report to the SCAQMD, ENVIRON International Corp., 101 Rowland Way, Suite 220, Novato, CA 94945.

Fan H, Sailor DJ, 2005. Modeling the Impacts of Anthropogenic Heating on the Urban Climate of Philadelphia: A comparison of implementations in two PBL schemes. Atmospheric Environment, 39, 73-84.

Fann N, Brennan T, Dolwick P, Gamble JL, Ilacqua V, Kolb L, Nolte CG, Spero TL, Ziska L, 2016. Air Quality Impacts. Chapter 3 in: *The Impacts of Climate Change on Human Health in the United States: A Scientific Assessment.* U.S. Global Change Research Program, Washington DC, 69–98. doi: 10.10.7930/J0GQ6VP6.

Founda D, Santamouris M, 2017. Synergies between urban heat island and heat waves in Athens (Greece) during extremely hot summer (2012). Scientific Reports, 7: 10973. doi:10.1038/s41598-017-11407-6.

Herrera M, Natarajan S, Coley, DA, Kershaw T, Ramallo-Gonzalez AP, Eames M, Fosas D, Wood M, 2017. A review of current and future weather data for building simulation, Journal of Building Services Engineering Research and Technology, 38, 602-627 doi: 10.1177/0143624417705937.

Hess JJ, Saha S, Schramm PJ, Conlon KC, Uejio CK, Luber G, 2018. Projecting climate-related disease burden: A guide for health departments. Climate and health technical report series, Centers for Disease Control and Prevention.

Hong T, Muehleisen R, Long N, New JR, 2017. Seminar 43 - Urban-Scale Energy Modeling, Part 3. *Proceedings of the ASHRAE Winter Conference*, Las Vegas, NV, January 31, 2017.

Hong T, Chen Y, Lee SH, Piette MA, 2016. CityBES: A web-based platform to support city-scale building energy efficiency. Urban Computing, August 14, 2016, San Francisco, California.

Houghton A, English P, 2014. An approach to developing local climate change environmental public health indicators, vulnerability assessments, and projections of future impacts. Journal of Environmental and Public Health, doi: 10.1155/2014/132057.

Huang YJ, 2016. How much do HVAC loads change due to the variability of year-to-year weather? ASHRAE Annual Conference, 2016, St. Louis, MO.

Huang J, 2010. Updating Energy Commission standard weather data for use in California building energy efficiency standards. Workshop on the 2013 Building Energy Efficiency Standards, November 16, 2010, California Energy Commission, Sacramento, California.

Jentsch MF, Eames ME, Levermore GJ, 2015. Generating near-extreme summer reference years for building performance simulation. Journal of Building Services Engineering Research and Technology 36, 503-522.

Kusaka H, Kondo H, Kikegawa Y, Kimura F, 2001. A simple single-layer urban canopy model for atmospheric models: Comparison with multi-layer and slab models. Boundary-Layer Meteorology, 101, 329-358.

Martilli A, Clappier A, Rotach MW, 2002. An urban surface exchange parameterization for mesoscale models. Boundary-Layer Meteorology, 104, 261-304.

Mylona A, 2012. The use of UKCP09 to produce weather files for building simulation. Journal of Building Services Engineering Research and Technology, 33, 51-62.

Nair RJ, Brembilla E, Hopfe C, Mardaljevic J, 2020. Weather data for building simulation: Grid resolution for climate zone delineation. Proceedings of Building Simulation 2019: 16th Conference of IBPSA, Rome, Italy, 2nd-4th September 2019, pp.3932-3939

New JR, Bhandari M, Shrestha S, Allen MR, 2018. Creating a virtual utility district: Assessing quality and building energy impacts of microclimate simulations, *International Conference on Sustainable Energy and Environment Sensing, Cambridge UK, June 18-19, 2018.*

Salamanca F, Martilli A, 2009. A new building energy model coupled with an urban canopy parameterization for urban climate simulations – Part II: Validation with one-dimension off-line simulations. Theoretical and Applied Climatology, 99, 345-356, doi: 10.1007/s00704-009-0143-8.

Skamarock W, Klemp J, Dudhia J, et al., 2008. A description of the Advanced Research WRF. NCAR Technical Note NCAR/TN-475+STR, National Center for Atmospheric Research, Boulder, Colorado.

Sleeter BM, Wilson TS, Sherba JT, 2017a. Land use and land cover projections for California's 4th Climate Assessment. US Geological Survey Data Release, doi: 10.5066/F7M61HFP. IP-083329.

Sleeter BM, Wilson TS, Sharygin E, Sherba JT, 2017b. Future scenarios of land change based on empirical data and demographic trends. Earth's Future, 5, 1068–1083, doi: 10.1002/2017EF000560.

Taha H, 2020a. Intra-urban enhancements to probabilistic climate forecasting for the electric system. Contract EPC-15-070 Report prepared for the California Energy Commission. To be published online on the California Energy Commission website (https://www.energy.ca.gov/energy-rd-reports-n-publications).

Taha H, 2020b. Capital Region Heat Pollution Reduction: Atmospheric Modeling for the Development of a Regional Heat Pollution Reduction Plan. Project Report prepared for the Sacramento Metropolitan Air Quality Management District for Contract LGC 299. http://www.airquality.org/LandUseTransportation/Documents/Altostratus_Final_Report.pdf.

Taha H, 2017. Characterization of urban heat and exacerbation: Development of a heat island index for California. Climate 5, 59. doi:10.3390/cli5030059.

Taha H, 2015a. Cool cities: counteracting potential climate change and its health impacts. Current Climate Change Reports, doi: 10.1007/s40641-015-0019.

Taha H, 2015b. Meteorological, air-quality, and emission-equivalence impacts of urban heat island control in California. Invited Paper, Sustainable Cities and Society, doi: 10.1016/j.scs.2015.03.009.

Taha H, 2008a. Meso-urban meteorological and photochemical modeling of heat island mitigation. Atmospheric Environment, 42, 8795-8809, doi:10.1016/j.atmosenv.2008.06.036.
Taha H, 2008b. Episodic performance and sensitivity of the urbanized MM5 (uMM5) to perturbations in surface properties in Houston TX. Boundary-Layer Meteorology 127, 193-218, doi:10.1007/s10546-007-9258-6.
Taha H, 2008c. Urban surface modification as a potential ozone air-quality improvement strategy in California: A mesoscale modeling study. Boundary-Layer Meteorology, 127, 219-239, doi:10.1007/s10546-007-9259-5.
Taha H, Levinson R, Mohegh A, Gilbert H, Ban-Weiss G, Chen S, 2018a. Air-temperature response to neighborhood-scale variations in albedo and canopy cover in the real world: Fine-resolution meteorological modeling and mobile temperature observations in the Los Angeles climate archipelago. Climate 6, 53 (25 pp), doi: 10.3390/cli6020053.
Taha H, Ban-Weiss G, Chen S, Gilbert H, Goudey H, Ko J, Mohegh A, Rodriguez A, Slack J, Tang T, Levinson R, 2018b. Modeling and observations to detect neighborhood-scale heat islands and inform effective countermeasures in Los Angeles. California's Fourth Climate Change Assessment, California Energy Commission, publication number CCCA4-CEC-2018-007.
Tesche TW, McNally DE, Emery CA, Tai E, 2001. Evaluation of the MM5 model over the Midwestern U.S. for three 8-hour oxidant episodes, Prepared for the Kansas City Ozone Technical Workgroup. Alpine Geophysics LLC.